Prediction of 475°C embrittlement in stainless steel welds using phase field model†

SAIDA Kazuyoshi * and NISHIMOTO Kazutoshi *

KEY WORDS: (475°C embrittlement) (Austenitic stainless steel) (Spinodal decomposition) (Phase field model) (Prediction of hardening) (Computer simulation) (Solidification mode)

1. Introduction

It has been widely recognised that ferritic stainless steels with more than 20mass%Cr are embrittled by exposure to temperature of 673-823 K known as "475°C embrittlement". This embrittlement is generally attributed to the separation of an originally single phase to one containing an iron-rich bcc phase (α) and a chromium-rich bcc phase (α') caused by spinodal decomposition. On the other hand, the chemical compositions of the austenitic stainless steel weld metals have been designed to contain the 3-10vol% ferritic phase in order to reduce the hot cracking susceptibility.

The objective of the present study is to validate the possibility of spinodal decomposition in the austenitic stainless steel weld metal. The effect of alloying elements in a ferritic phase, which is influenced by the solidification mode, on the behaviour of spinodal decomposition was investigated by the computer simulation based on the phase filed model for ternary alloy system.

2. Materials and Experimental Procedures

Austenitic stainless steels used in the present study are three kinds of type 316L stainless steels with the slightly different chemical compositions within a standard. The chemical compositions of steels used were shown in **Table 1**. In order to obtain the weld metal of type 316L stainless steels, GTA melt-run welding was conducted.

Table 1 Chemical compositions of steels used (mass%)

Steel	C	Si	Mn	P	S	Cr	Ni	Mo	N	Fe
SUS316L-1	0.014	0.58	0.96	0.025	0.005	18.00	12.3	2.03	0.024	Bal.
SUS316L-2	0.016	0.55	1.18	0.029	0.012	16.38	12.44	2.10	0.024	Bal.
SUS316L-3	0.019	0.35	1.34	0.011	0.005	18.70	11.40	2.12	0.030	Bal.

3. Microstructural Analysis of Weld Metals

Figure 1 shows the SEM microstructures of the melt-run weld metals of type 316L-1 and type 316L-2 stainless steels. In case of the type316L-1 weld metal, a vermicular or lathy ferritic phase is located mainly at the axes of the cells or dendrites, its solidification mode being determined as FA mode. A ferritic phase is located at cellular dendritic substructure boundaries in the type 316L-2 weld metal, its solidification mode being determined as AF mode. **Table 2** shows the measured chemical compositions of a ferritic phase in the weld metals with FA mode (type 316L-1) and AF mode (type 316L-2). Nevertheless the content of Cr in the base metal of type 316L-1 stainless steel is higher than that of type 316L-2, and the contents of Ni and Mo are comparable in each base metal, the contents of Cr, Mo and Ni in a ferritic phase with AF mode are higher than those with FA mode. It follows that alloying elements of Cr, Ni and Mo are relatively enriched in a ferritic phase with AF mode compared with that with FA mode.

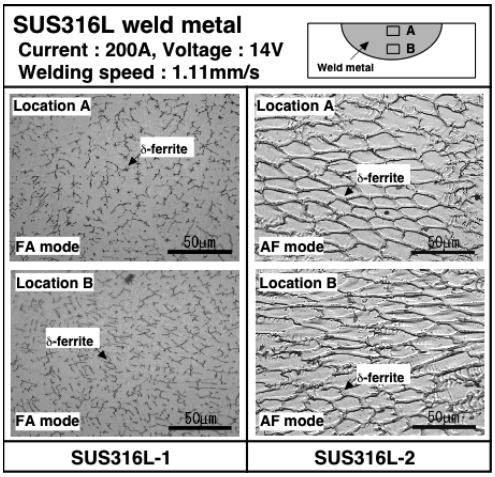

Fig. 1 Comparison of microstructure in weld metal between SUS316L-1 and SUS316L-2

Table 2 Analysed compositions of δ-ferrite (at%)

δ-ferrite	Fe	Cr	Mo	Ni
FA mode	64.3	28.1	2.5	5.1
AF mode	57.2	29.4	6.2	7.2

† Received on 30 September 2010

* Dept. of Materials & Manufacturing Science,.Graduate School of Eng., Osaka University, Osaka, Japan

Transactions of JWRI is published by Joining and Welding Research Institute, Osaka University, Ibaraki, Osaka 567-0047, Japan

4. Computer Simulation of Spinodal Decomposition

Phase Field Model of Spinodal Decomposition for Ternary Alloys

The evaluation equations governing spinodal decomposition in the *A-B-C* ternary system are expressed as:

$$\frac{\partial c_2}{\partial t} = \nabla \cdot \left(L_{22} \nabla \frac{\delta G_{sys}}{\delta c_2} + L_{23} \nabla \frac{\delta G_{sys}}{\delta c_3} \right)$$
$$\frac{\partial c_3}{\partial t} = \nabla \cdot \left(L_{32} \nabla \frac{\delta G_{sys}}{\delta c_2} + L_{33} \nabla \frac{\delta G_{sys}}{\delta c_3} \right) \quad (1)$$

where c_i is the local composition of the component i at spatial position **r** (**r** represents a vector) and time t in the microstructure. The subscript numbers i = 1, 2 and 3 refer to elements *A*, *B* and *C*, respectively. G_{sys} is the total free energy of the microstructure, which is expressed by the sum of the Gibbs energy density, the density of the composition gradient energy and the density of the elastic strain energy. L_{ij} is the Onsager coefficient.

In the present study, it is assumed that the change in hardness due to spinodal decomposition and/or 475°C embrittlement is followed by the precipitation hardening theory (cut-through model) proposed by Mott-Nabarro.

Effect of Alloy Composition on Spinodal Decomposition

The microstructure evolution in Fe-Cr-Mo ternary alloy was calculated. **Figure 2** shows the two-dimensional profiles of Fe, Cr and Mo concentrations perpendicular to the direction [001] of α phase during isothermal spinodal decomposition at 723 K. The original single phase is phase-decomposed into Fe-rich (α) and Cr-rich (α') phases with the progress of ageing. In the initial stage of spinodal decomposition, Mo is distributed along with Fe in the α phase. Then, the bifurcation of Mo peaks along peak tops of Cr concentration occurs with the progress of phase decomposition. Then, Cr-rich α' phase grows and coarsens as well as slightly modulating along <100> direction with the lapse of ageing time. Mo is finally redistributed to the interface between α and α' phases, and surrounds Cr-rich α' phase.

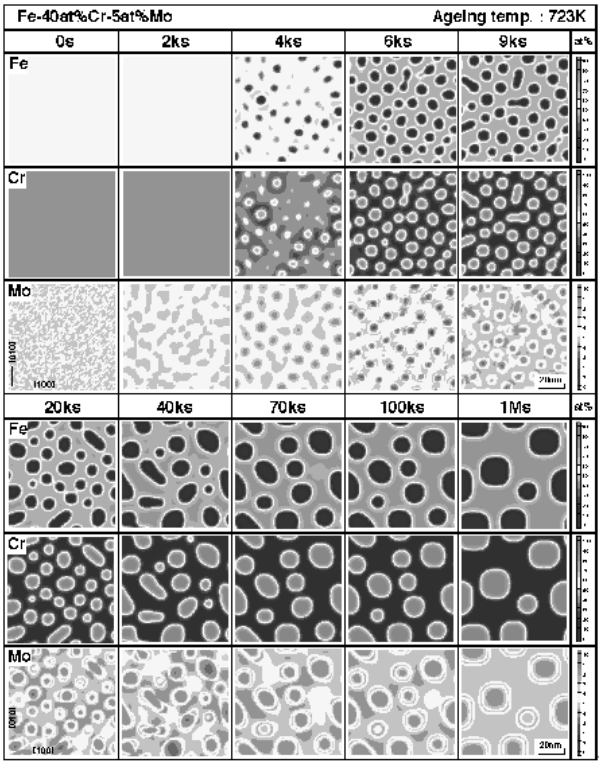

Fig. 2 Time evolution of spinodal decomposition calculated for Fe-40at%Cr-5at%Mo alloy

The effects of Cr and Ni contents in Fe-Cr-Ni ternary alloy on the beginning time for spinodal decomposition were investigated. **Figure 3** shows the predicted contour of the beginning time for spinodal decomposition as the function of Cr and Ni compositions. The beginning time for spinodal decomposition shortens with increasing Cr composition, while it much lengthens contrarily with increasing Ni composition. Furthermore, it takes extremely long time to spinodal-decompose with the chemical compositions of the alloy approaching the spinodal line. The result is that spinodal decomposition would be delayed in approx. half or one order of time when Ni composition is varied in 1at%.

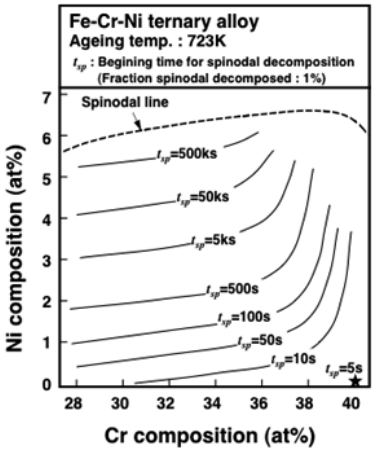

Fig. 3 Contour of beginning time for spinodal decomposition in Fe-Cr-Ni ternary alloy

Prediction of Hardening due to Spinodal Decomposition

The hardening behaviour of a ferritic phase due to spinodal decomposition was predicted. **Figure 4** shows the predicted Martens' hardness increment ΔHM of a ferritic phase with different solidification modes during spinodal decomposition process. The hardness of a ferritic phase with FA mode begins to increase at the holding time approx. 5 Gs, while that with AF mode begins to increase at the holding time as long as approx. 150 Gs. It follows that the hardening and/or 475°C embrittlement due to spinodal decomposition of a ferritic phase with FA mode would take place more rapidly compared with AF mode, and that the maximum hardness increment attained with a ferritic phase with AF mode is slightly higher than that with FA mode.

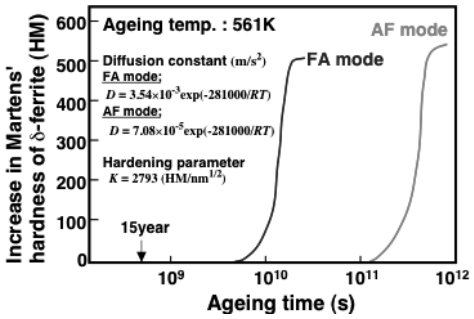

Fig. 4 Prediction of hardening in ferritic phase with different solidification modes due to spinodal decomposition at 561K

5. Conclusions

(1) The original single phase was phase-decomposed into Fe-rich and Cr-rich phases with the progress of ageing. The beginning time for spinodal decomposition shortened with increasing Cr composition, while it much lengthened contrarily with increasing Ni composition.

(2) The predicted hardness of a ferritic phase with FA mode began to increase as the holding time approx. 5 Gs, while that with AF mode began to increase at the holding time as long as approx. 150 Gs.